Adsorbates on Gd(0001): A combined scanning tunneling microscopy and photoemission study

Mathias Getzlaff, Matthias Bode, Rene Pascal, and Roland Wiesendanger
Institute of Applied Physics and Microstructure Research Center, University of Hamburg, Jungiusstrasse 11, D-20355 Hamburg, Germany

(Received 3 February 1998; revised manuscript received 29 June 1998)

We report on the electronic structure of hydrogen, oxygen, and carbon monoxide on Gd(0001), and the development of adsorption processes studied by means of photoelectron spectroscopy in combination with scanning tunneling microscopy and spectroscopy, respectively. Due to its high spatial resolution, the *visualization* of the adsorption process is obtained. For hydrogen, it was found that the adsorption occurs in two steps. It starts at crystallographic surface imperfections. From these nucleation centers, a domainlike spreading is present which is strongly hindered at surface steps. Oxygen on the Gd monolayer possesses an ordered structure which could be determined to be $(2\sqrt{3}\times 2\sqrt{3})R30°$. Carbon monoxide adsorbs molecularly at low temperatures and dissociatively at room temperature. The adsorption process of a hydrogen-covered Gd film being exposed to carbon monoxide consists of five steps. At the beginning the whole amount of adsorbed hydrogen atoms is removed from the surface. In the intermediate regime, carbon and oxygen is adsorbed at or near the surface. The last step demonstrates the oxidation to Gd_2O_3 acting as a catalyst for the transformation of CO to CO_2 which creates stable carbonate species at the surface. This formation also occurs for the adsorption of oxygen and carbon monoxide. [S0163-1829(99)07411-1]

I. INTRODUCTION

Rare-earth metals are of great scientific interest because of unusual electronic and magnetic properties which arise from their highly localized $4f$ electrons. A detailed knowledge about the electronic structure of the surface is essential to understand the mechanisms responsible for surface magnetic order. Over the past decade the extraordinary surface magnetic properties of heavy rare-earth metals have been a subject of growing interest, and, as described below, some results are still highly controversial.

Gd(0001) is considered to be the prototype ferromagnet among lanthanides with localized magnetic moments. A magnetic surface state which was shown to be spatially localized with a d_{z^2}-like orbital symmetry was made responsible for the enhancement of the surface Curie temperature T_C^{surf} by up to 60 K (Refs. 1–3) compared to the bulk Curie temperature of 293 K. Whereas in the past an antiferromagnetic coupling between bulk and surface was experimentally observed[1] and theoretically supported,[4] it is nowadays widely believed that the surface state and the surface $4f$ states couple ferromagnetically to the bulk magnetic moments.[5] The oscillatory behavior between ferromagnetism and antiferromagnetism used in the description of the Ruderman-Kittel-Kasuya-Yusida interaction depends strongly on the atomic distance. The controversial findings mentioned above may therefore be explained by a small shift of the outermost interlayer spacing. Relatively thick films show a canted magnetization.[6,7] The influence of adsorbates on single-crystal surfaces provides valuable insights into the surface electronic structure, and thus a better understanding of the surface magnetism in the rare-earth metals.

Adsorbates can significantly alter the electronic structure of the underlying substrate, and are additionally of great importance in technological processes, e.g., heterogeneous catalysis. In the past, only a small number of investigations on adsorbates like hydrogen,[8] oxygen,[9–16] and carbon monoxide[17] on rare-earth metal surfaces have been carried out due to the difficulty in preparing atomically clean and well-ordered surfaces showing a characteristic surface state near the Fermi level. Previous studies have been performed on Gd(0001),[18–21] Tb(0001),[21,22] Nd(0001),[23] and Pr(0001).[24] Some investigations were carried out on bulk crystals, but thin films on nonmagnetic substrates prevail in today's experiments.

Here we report on the investigation of the electronic structure of hydrogen, oxygen, and carbon monoxide being adsorbed on Gd(0001)/W(110) by means of photoelectron spectroscopy. The combination with scanning tunneling microscopy and spectroscopy enables one to determine the spatially resolved local density of states for the adsorbates and the clean Gd(0001) film as well as the *visualization* of the adsorption process which can be carried out on the same sample. Hydrogen adsorption shows a two-step behavior; the adsorption begins at surface imperfections which are the starting points for a domainlike spreading which is strongly hindered at crystallographic surface imperfections. Oxygen and carbon monoxide adsorb dissociatively with the creation of a subsurface oxide, and subsequently with oxidation. In order to obtain a deeper insight into the understanding of heterogeneous catalysis, the adsorption process of hydrogen-covered Gd films exposed to CO was determined. It consists of five steps, with the first ones characterized by a total removal of the adsorbed hydrogen atoms.

II. EXPERIMENTAL DETAILS

For a determination of the electronic structure, angle-resolving photoelectron spectroscopy was used. Photoelectrons were produced by linearly polarized vacuum ultraviolet

radiation from a discharge lamp (Ne I resonance line $h\nu = 16.85$ eV) with a triple-reflection polarizer using an improved version of the system described in Ref. 25. The angle of the incoming photon beam was $\theta_{ph} = 45°$ with respect to the surface normal. A cylindrical mirror analyzer with sector field (300-mm slit-to-slit distance) and high transmission served as the energy dispersing element with the additional angular resolution of the photoelectrons (acceptance cone $\pm 3°$). The overall energy resolution was set to about 300 meV. The experiment was performed in a μ-metal UHV chamber to provide magnetic shielding, and the base pressure was below 3×10^{-11} mbar. It is equipped with a combined low-energy electron-diffraction (LEED)/Auger system for surface characterization. An *in situ* transfer between the ultraviolet photoemission spectroscopy stage and scanning tunneling microscopy (STM) enables one to investigate the *same* sample.

The topography was measured in the constant current mode with a commercial scanning tunneling microscope with cut Pt/Ir tips. In order to determine the dI/dU signal by the lock-in technique, the feedback circuit was switched off, and an ac component ($U_{\mathrm{mod}} \leqslant 20$ mV, $\nu \approx 325$ Hz) was added to the gap voltage U. The stabilization parameters before each spectroscopy curve were typically set to about 0.8 V and 0.2–0.5 nA. Since the tunneling current I was recorded simultaneously with the dI/dU signal, we were able to quantify the latter in units of nanoampere per volt instead of arbitrary units.

A W(110) crystal served as substrate for the growth of Gd films. It was cleaned by heating in oxygen and flashing up to 2600 K. The Gd films were deposited by means of an electron-beam evaporator using tungsten crucibles. The growth rate was typically set to 0.5 layer per minute. The preparation procedure was based on the investigations by Aspelmeier, Gerhardter, and Baberschke.[26] The experiments were performed on two different kinds of samples. Smooth Gd(0001) films were prepared by evaporation of more than 30 ML with the substrate held at room temperature, and subsequent annealing at 700 K for 2 min. For coverages less than 10 ML, we observed Stranski-Krastanov island formation; between the islands a monolayer of Gd covered the tungsten substrate as described by Tober *et al.*[27] During Gd deposition the pressure stayed below 3×10^{-10} mbar. The surface was exposed to hydrogen, oxygen, and carbon monoxide by means of a high-precision leak valve. The amount is characterized in Langmuir ($1\ \mathrm{L} = 10^{-6}$ torr s) and not corrected by the ion gauge correction factor.

III. RESULTS AND DISCUSSION

The investigations were performed on atomically clean and well-ordered hcp(0001) Gd surfaces prior to the exposure of hydrogen, oxygen, and carbon monoxide, as indicated by the existence of the Gd surface state.

For the photoemission investigation, smooth Gd(0001) films were prepared and subsequently exposed. STM investigations showed[28] that the Gd surface state exists both on smooth films and multilayer Gd islands. Multilayer island films were additionally chosen for the STM investigations to provide topographical contrast in order to distinguish between sample states and tip-induced artifacts as well as to determine the influence of different island heights. The detailed preparation procedure was described above.

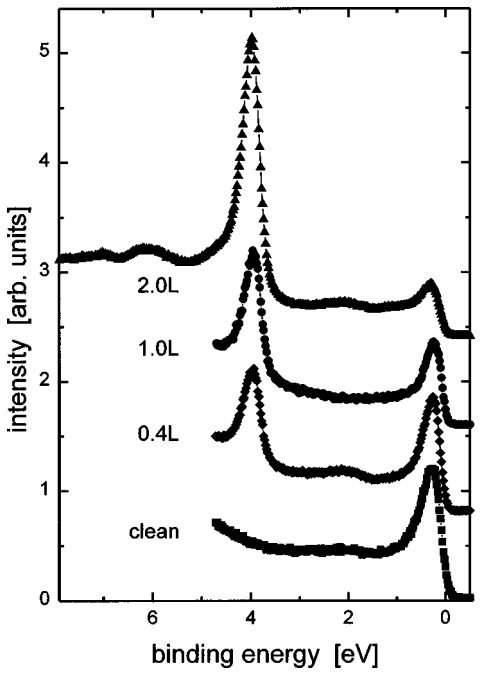

FIG. 1. Photoemission spectra at normal emission for different hydrogen exposures on Gd(0001)/W(110). The photon energy is 16.85 eV.

A. Exposing Gd(0001) to hydrogen

Photoelectron spectra from the clean Gd(0001) surface and hydrogen exposures are shown in Fig. 1. The spectra are taken in normal emission and at room temperature. The sharp feature near the Fermi edge is due to the clean Gd(0001) surface state and is only observed on contamination-free high-quality hcp(0001) surfaces. Our high-quality LEED pattern showed a hexagonal structure with sharp spots on a low background.

After hydrogen exposure a pronounced feature at a binding energy of about 4 eV appears. The energy width (full width at half maximum) of this H-induced state is equal to 0.4 eV and similar to that of the surface state. The feature at about 2 eV is caused by Gd Δ_2 bulk bands.[29] Dosing additional hydrogen suppresses the Gd surface state as previously demonstrated by Li *et al.*[8]

As shown in the photoelectron spectra, the hydrogen-induced state has a binding energy of about 4 eV, and is therefore nearly unaccessible to STM investigations. It is nevertheless possible to resolve the spatial distribution of hydrogen since the suppression of the Gd surface state leads to a drastic reduction of the differential conductivity at low-bias voltages. This behavior is illustrated in Fig. 2 which shows the tunneling dI/dU spectra (stabilization parameters $U = 1.0$ V, $I = 0.3$ nA) measured on Gd(0001) island surfaces (solid curve), on the first Gd monolayer between the islands (dash-dotted line), and on areas which have been modified by hydrogen adsorption (dashed line). The suppression of the exchange-split Gd(0001) surface state with its predominantly majority character in the occupied part[5] and predominantly minority character in the unoccupied band

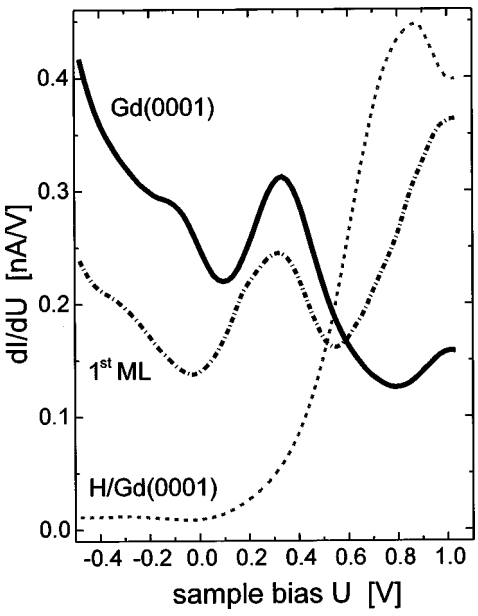

FIG. 2. Tunneling dI/dU spectra (stabilization parameters: $U=1.0$ V, $I=0.3$ nA) measured on Gd island surfaces (solid), on the first Gd monolayer between the islands (dash-dotted line), and on areas which have been affected by hydrogen adsorption (dashed line).

part[30] can be clearly seen. The strong decrease in the differential conductivity which is essentially proportional to the local density of states at the surface demonstrates the strong geometrical localization of the surface state; bulk states do not show such pronounced differences. The tunneling spectra reveal that for the Gd monolayer only one peak at about 0.3 V is present (see Fig. 2) which cannot be attributed to the surface state. This can be deduced from the observation that no changes in the tunneling spectra occur after hydrogen adsorption. A surface state, in contrast, is very sensitive to adsorbates (cf. Fig. 1). Additionally, the determination of the energies of both spin counterparts from the surface state as a function of temperature showed a shift toward the Fermi level; the feature of the monolayer, however, remained fixed in energy.[28] Therefore, hydrogen adsorption does not significantly modify the electronic structure of the monolayer close to the Fermi level. The lattice mismatch between bulk Gd and thin Gd films decreases with increasing thickness.[31] The exchange splitting of the Gd surface state increases with increasing film thickness and remains constant from 4 ML upwards.[32] Consequently, the 2- and 3-ML-high islands have a modified surface in comparison to bulk hcp(0001), which cause differences in the adsorption process.

In Figs. 3(a) and 3(b), constant-current topographs ($U=-0.3$ V, $I=0.03$ nA) of Gd islands on W(110) are shown after different hydrogen exposures. Between the high Gd islands which have a (0001) surface, there is a Gd monolayer covering the tungsten substrate. In addition, 2- and 3-ML-high islands are to be seen. The steps of the tungsten substrate remain visible on the high Gd islands. The lines arise from lattice dislocations through the whole island due to different lattice constants in perpendicular direction.

Figure 3(a) shows this system after an exposure of 0.2-L hydrogen. The Gd(0001) monolayer and the low islands remain nearly unaffected. The monolayer of Gd on W(110)

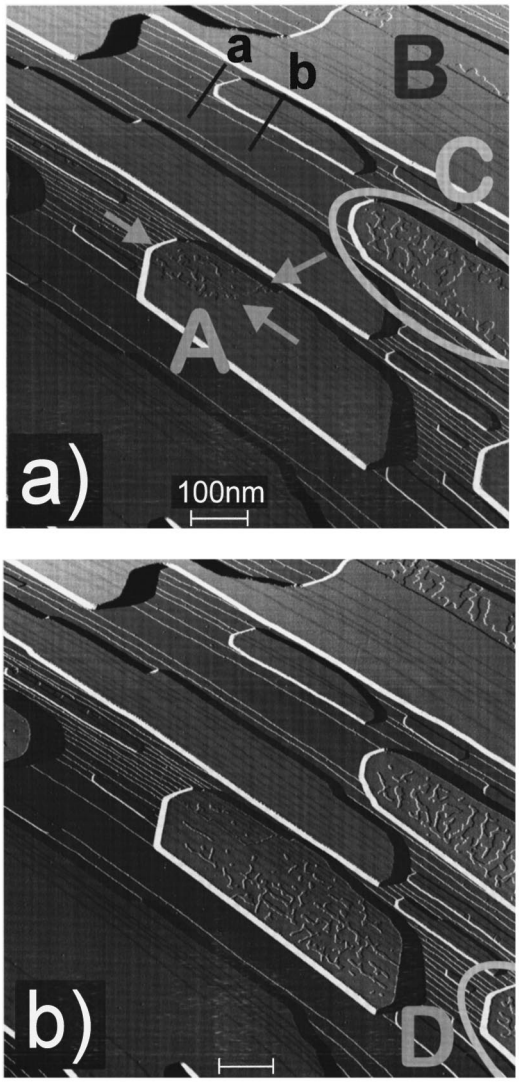

FIG. 3. Constant-current topograph ($U=-0.3$ V, $I=0.03$ nA) of Gd islands on W(110). Between high Gd islands with a (0001) surface, a Gd monolayer covers the tungsten substrate. Additionally, 2- and 3-ML-high islands are to be seen. (a) To this system, 0.2-L hydrogen was dosed. (b) The same area as in (a), but with an additional dosage of 0.8 L resulting in a total amount of 1.0-L hydrogen.

possesses a strained hcp structure with a dilatation of about 8%.[31] On top of the high islands, two different kinds of behaviors can be observed. Some of them show a smooth surface which is undisturbed by the hydrogen. Others present a lagoonlike appearance of alterations. In the regions with a ''collapsed'' appearance, the Gd(0001) surface state is suppressed, whereas in the unaltered regions it still exists. Due to the reduction in the differential conductivity of the hydrogen-covered areas, the tip has to move toward the surface in order to maintain a constant current. The change in appearance is not a topographical effect, but is mainly caused by the modification in the electronic structure, namely, the suppression of the Gd surface state.

The special behavior of the adsorption process may be understood by examining the areas which are labeled *A*, *B*, and *C*. In region *A* there are lattice dislocations even for the clean Gd surface which are marked by arrows (more easily

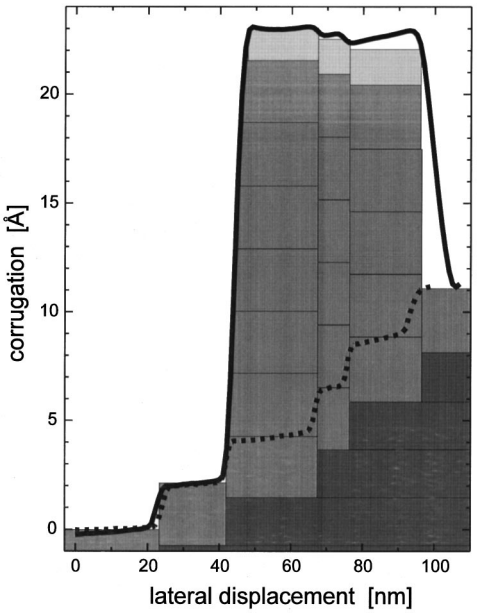

FIG. 4. Line section [see lines *a* and *b* in Fig. 3(a)] of a Gd island (solid line) and the Gd monolayer on top of the tungsten substrate (dotted line). Tungsten is marked by dark gray, Gd(0001) by gray, and the electronic height due to the surface state by light gray shaded areas. In order to minimize the surface energy the Gd island tries to create a flat surface, resulting in an inverted step height behavior on top of the island.

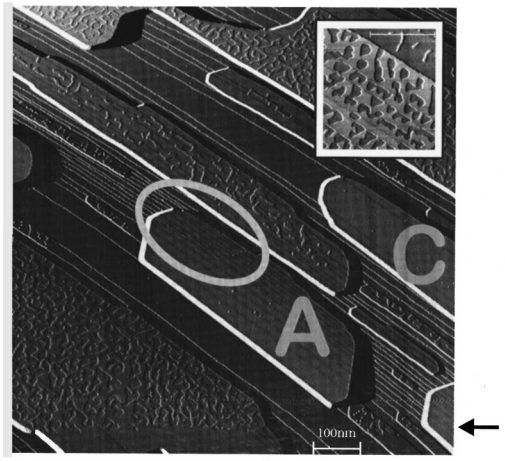

FIG. 5. The same area as in Fig. 3. At the beginning of the scan (bottom), the dosage was 1.6 L. During the scan, 1 L of hydrogen was additionally offered (marked by the black arrow). Unconnected areas are more easily to be seen in the enlarged image (see inset).

seen in Fig. 5, marked by the ellipse). These are the starting points for the adsorption process. In region *B* it can be observed that the spreading of the adsorption is strongly suppressed at step edges due to surface steps on the tungsten substrate. The further evolution of this process is demonstrated in region *C*. Once the adsorption of hydrogen has started, then the suppression of the surface state extends over the whole area. This behavior is also shown in Fig. 3(b). It is the same area as in Fig. 3(a) but with an additional exposure of 0.8 L, resulting in a total amount of 1.0-L hydrogen. The areas which were already affected after 0.2 L have been spread out. Additionally, the adsorption occurred on a further island (region *D*). For a comparison with results obtained by photoelectron spectroscopy, one should keep in mind that the photoemission experiment averages over these regions; thus both the peak of the Gd surface state and the hydrogen-induced feature are coexistent, as observed in the spectra in Fig. 1.

The adsorption of hydrogen seems to occur in two steps. Hydrogen is first adsorbed at surface imperfections, and, second, starting from these points, the adsorption spreads out to the step edges, which form boundaries strongly hindering the further process. The steps of the tungsten substrate are even visible on top of the Gd islands. This observation is caused by the different heights of the W(110) and Gd(0001) layer being 2.23 and 2.89 Å, respectively. Between the islands, the whole substrate is covered with a Gd monolayer; therefore, the step height of the monolayer is the same one as for W(110), as shown by the dotted line section in Fig. 4, which corresponds to line *a* in Fig. 3(a). The solid line section [cf. line *b* in Fig. 3(a)] demonstrates the inverted step height behavior on top of the Gd island, i.e., the tungsten terrace being one atomic layer higher appears lower on the island surface. An analogous observation was reported for Gd/W(100).[33] The surface of the island tries to be atomically flat in order to reduce its surface energy. Therefore, the height decreases from the left to the right from seven to five layers. To the ''topographic'' height (see gray shaded area) the ''electronic'' height of the surface state (see light gray shaded areas) being about 1.7 Å [cf. Fig. 7(c)] must be added. This is due to the large fade-out length into the vacuum accompanied with a relatively high local density of states above the surface. In the STM experiment operating in the constant-current mode, the tip therefore has to be moved upwards. The tungsten substrate is marked by dark gray shaded areas.

In Fig. 5, the same area as in Fig. 3 is shown. At the beginning of the scan (bottom), the total exposure so far was 1.6 L, dosed during the past 1 h. During the scan, the sample was exposed within a few seconds to an additional amount of 1 L (marked by the black arrow). Now, the islands containing regions *A* and *C* present a suppressed surface state on top of the whole island. The lattice dislocation already present in the clean Gd island is marked by an ellipse. The large island in the lower left corner shows the domainlike modification with the additional hydrogen exposure. After the additional exposure the whole island exhibits a suppression of the surface state. The exposure time for the additional 1 L of hydrogen was substantially shorter than the previous time for 1.6 L. This observation indicates that the adsorption process changes with the dosage. In order to determine the collision rate, one can estimate the fluence, i.e., the total number of collisions per unit surface area, by $p/\sqrt{2\pi m k_B T}$,[34] where p is the pressure, m the mass of a molecule, and T the temperature. Considering the ion gauge correction factor the collision rate at room temperature for 1 L is about 30 hydrogen molecules per nm^2. On the clean surface the presence of two or more hydrogen molecules *simultaneously* seems to be necessary to cause adsorption. This conclusion is corroborated by the observation that prior to the supplementary exposure of 1 L the hydrogen covered areas are connected but afterwards the additionally created regions are mainly isolated to each other (see inset). This means that on areas of

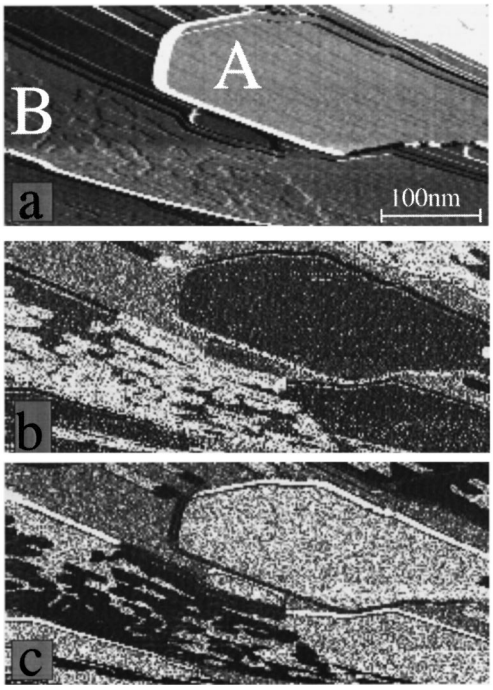

FIG. 6. (a) Topography of a Gd island system being exposed to hydrogen. The clean Gd surface is marked by *A*, the hydrogen affected island by *B*. (b) and (c) Maps of the differential conductivity dI/dU for a bias voltage of $U=0.7$ V in (b) and $U=-0.3$ V in (c) are coded gray. The bright areas in the lower part are caused by hydrogen-covered areas (b), whereas they appear dark for negative voltages (c). This behavior is obvious in connection with the dI/dU spectra in Fig. 2.

the surface being clean and of high crystallographic order the adsorption of hydrogen cannot be carried out via a spreading process, but only by a simultaneous presence of at least two hydrogen atoms. On the Gd(0001) monolayer no alterations can be observed. Significant modifications take place on the low islands as will be shown below.

Figure 6(a) shows the topography of approximately 5-ML Gd evaporated on the W(110) substrate held at 530 K. Since the Gd islands are atomically flat and the substrate exhibits several one-atomic steps below the island surface, the local coverage Θ_{loc} decreases for every island from the left toward the right edge. Simultaneously with the topography, we have measured the dI/dU spectrum at every pixel of the scan. Figures 6(b) and 6(c) show maps of the differential conductivity dI/dU for different sample biases: (b) $U=+0.7$ V and (c) $U=-0.3$ V. The differential conductivity is grey-coded, i.e., the higher the local dI/dU signal the brighter a location appears. At a sample bias $U=+0.7$ V the tunneling current is dominated by electrons which tunnel from the tip into unoccupied sample states with a binding energy of $+0.7$ eV. Comparison with the topographic data of Fig. 6(a) reveals that at this particular binding energy the differential conductivity above the Gd monolayer is higher than above those parts of the islands which have not been affected by hydrogen. Besides a few small bright pixels, the dI/dU signal measured above the Gd island is uniform, and therefore independent of the local coverage. In the dI/dU maps we never found a contrast on the Gd island at any sample bias [cf. Figs. 6(b) and 6(c)] in the voltage range under study

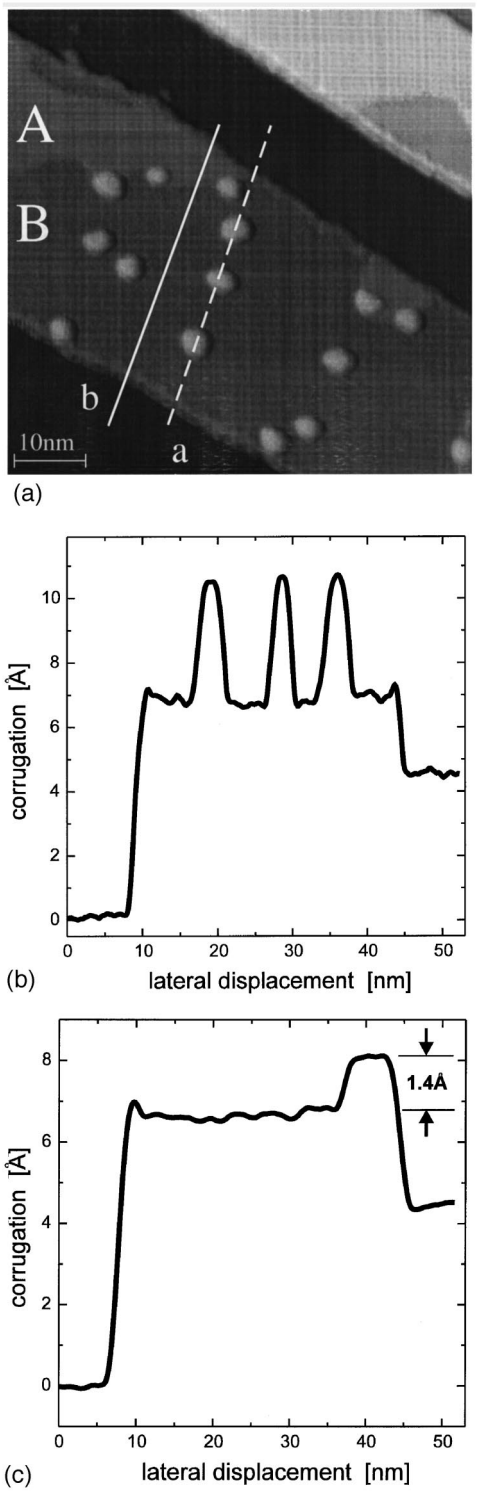

FIG. 7. (a) Constant-current topograph ($U=-0.3$ V, $I=0.03$ nA) for an enlarged image of a 3-ML-high Gd island on W(110) after an hydrogen exposure of 1.6 L, and subsequently of 1 L (cf. Fig. 5). Clean Gd is marked by *A*, the hydrogen-affected areas by *B*. (b) Line section of the clusters [see line *a* in (a)]. The width and the height are nearly uniform, and amount to 35 and 4 Å. respectively. (c) The suppression of the surface state due to hydrogen adsorption results in a collapsed looking area. The depth of this electronically induced depression amounts to about 1.4 Å, as obvious via the line scan [see line *b* in (a)].

(-0.6 V$\leqslant U\leqslant+0.9$ V). A high contrast occurs for island *B* in the lower part of the image. The bias voltage of 0.7 V was chosen due to the large differential conductivity for hydrogen-covered areas (cf. Fig. 2). The bright parts in Fig. 6(b) are therefore areas which have been affected by hydrogen. The dark appearance of the island *A* in the upper right part points to a clean surface. The tunneling spectra reveal (see Fig. 2) that at a bias voltage of -0.3 V the differential conductivity for hydrogen-affected areas is significantly reduced. This inversion of the contrast is shown in Fig. 6(c), with black areas pointing to adsorbed hydrogen.

Figure 7(a) shows an enlarged image of a 3-ML-high Gd island corresponding to the system presented in Fig. 5. Only those areas on which hydrogen is already adsorbed exhibit small clusters. This observation may be explained by the onset of the formation of Gd(0001) hydride. These clusters are created after the supplementary short-duration high-exposure dose. The line section (line *a*) shows a uniform height of these clusters being about 4 Å [Fig. 7(b)]. The suppression of the Gd surface state caused by the hydrogen adsorption occurring as a collapsed region (labeled by *B*; the clean Gd surface is marked by *A*) is demonstrated by the line section in Fig. 7(c) [line *b* in Fig. 7(a)]. The depth of this only *electronically* induced suppression, already discussed above, amounts to 1.4 Å. This value is smaller than for the suppression on high Gd islands. The Gd surface state is even fully developed for at least 4-ML-high areas.[32] The island with a height of three atomic layers possesses a surface state with a reduced fade-out length into the vacuum. The suppression due to the hydrogen adsorption therefore seems to be smaller than for high Gd islands.

The question arises as to whether or not the former findings are specific for Gd islands, i.e., depend on the sample morphology, or are also characteristic for the element Gd(0001). Therefore, hydrogen adsorption was additionally investigated for thick smooth Gd films. In Fig. 8(a) this topography is shown after a hydrogen exposure of 0.3 L. Again, the adsorption starts at the step edges and surface imperfections. As for Gd islands, the affected areas are coherent [cf. Fig. 3(a)]. The hydrogen ''islandlike'' formation was also deduced in photoemission experiments for H/Gd(0001) (Ref. 8) and H/Be(0001) (Ref. 35) by a determination of peak heights from hydrogen-induced states as a function of dosage. Further exposure [3.6 L in Fig. 8(b)] demonstrates the same behavior in the adsorption process, namely, a lagoonlike appearance. After an amount of 9 L [Fig. 8(c)], nearly the whole Gd film is covered with hydrogen. These observations point to no significant differences in the adsorption process of hydrogen on islands on the one hand, and on smooth films on the other hand.

The influence of the bias voltage on the topography which is presented in a STM image is demonstrated in Fig. 9. At negative voltages [$U=-0.3$ V in Fig. 9(a)] the hydrogen-affected areas exhibit a reduced apparent height due to the drasticallly reduced local density of states (LDOS) (cf. Fig. 2). Using moderate positive bias voltages [($U=0.8$ V in Fig. 9(b)], it is possible to obtain equal apparent heights for the clean Gd(0001) surface and hydrogen-affected areas. This observation is caused by the drastic increase of the LDOS for hydrogen on Gd(0001) toward higher voltages, as already demonstrated in Fig. 2. For high positive voltages

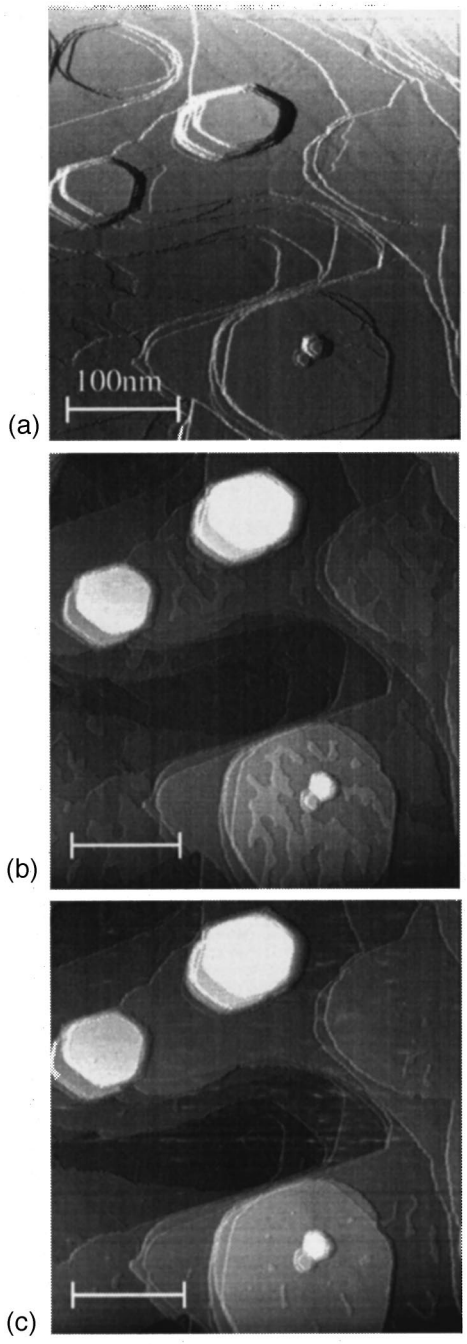

FIG. 8. Topography of a thick (about 40 ML) smooth Gd film being exposed to 0.3-L (a), 3.6-L (b), and 9-L (c) hydrogen. The adsorption starts at surface imperfections.

[$U=3.2$ V in Fig. 9(c)], an inversion of the corrugation (i.e., the hydrogen-affected areas now seem to be higher than for negative voltages), is present, as can be additionally deduced from the shape of the LDOS curves. Therefore, the depth of the so-called ''collapse'' [cf. Fig. 7(c)] is not uniform, and depends significantly on the bias voltage. This dependence can directly be determined in $z(U)$ measurements at a constant current.

These $z(U)$ measurements were obtained by scanning the sample bias at a constant tunneling current with the feedback left on, and measuring the z feedback signal versus the sample voltage. With the z calibration, obtained at mono-

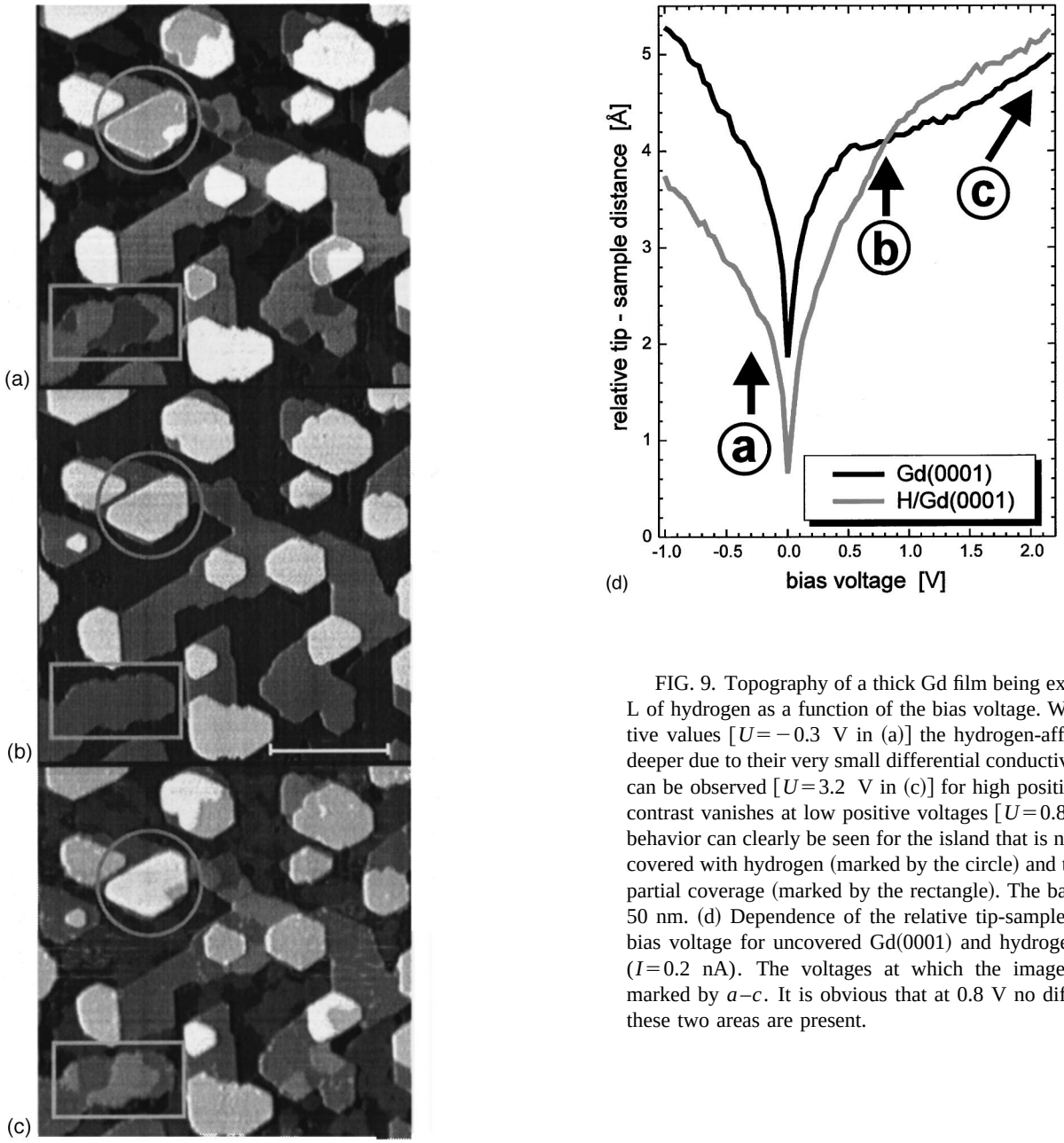

FIG. 9. Topography of a thick Gd film being exposed to about 1 L of hydrogen as a function of the bias voltage. Whereas for negative values [$U=-0.3$ V in (a)] the hydrogen-affected areas look deeper due to their very small differential conductivity, an inversion can be observed [$U=3.2$ V in (c)] for high positive voltages. The contrast vanishes at low positive voltages [$U=0.8$ V in (b)]. This behavior can clearly be seen for the island that is nearly completely covered with hydrogen (marked by the circle) and the region with a partial coverage (marked by the rectangle). The bar corresponds to 50 nm. (d) Dependence of the relative tip-sample distance on the bias voltage for uncovered Gd(0001) and hydrogen-affected areas ($I=0.2$ nA). The voltages at which the images are taken are marked by a–c. It is obvious that at 0.8 V no difference between these two areas are present.

atomic Gd(0001) steps, one obtains the relative tip displacement via the sample bias. The determination of the displacement was carried out in a current imaging mode at a region of the sample that consists of both clean Gd(0001) as well as hydrogen-covered areas. For each curve, about 50 measurements were averaged. Figure 9(d) shows the relative tip-sample distance as a function of the bias voltage for uncovered Gd(0001) and hydrogen-affected areas ($I=0.2$ nA). Those voltages at which the images are taken are marked, and correspond to the ones in Figs. 9(a)–(c). It is obvious that at negative and low positive bias voltages up to 0.8 V the hydrogen-affected areas exhibit a significantly reduced apparent height, whereas at higher positive voltages they appear a little bit higher than the clean Gd(0001) regions. At 0.9 V no differences between the two types of areas are present. The dependence on the bias voltage is clearly seen in the areas which are marked by a circle, presenting an island which is nearly completely covered with hydrogen and a rectangle showing a partial affected island, respectively.

It was shown (cf. Fig. 7) that after a short-duration, high-exposure, dose of hydrogen, small clusters are created on thin Gd islands. An analogous procedure was carried out on smooth films. Figure 10(a) shows this sample after a dosage of 10 L. Again, these clusters were created (see circle). It should be emphasized that most of these clusters are arranged as linear chains. A line section through these clusters is presented in Fig. 10(b). The height is uniformly about 4 Å, which is the same value as for clusters on thin films [cf. Fig. 7(b)]. The width being estimated by the full width at half maximum amounts to about 35 Å, also in agreement with hydrogen on thin islands.

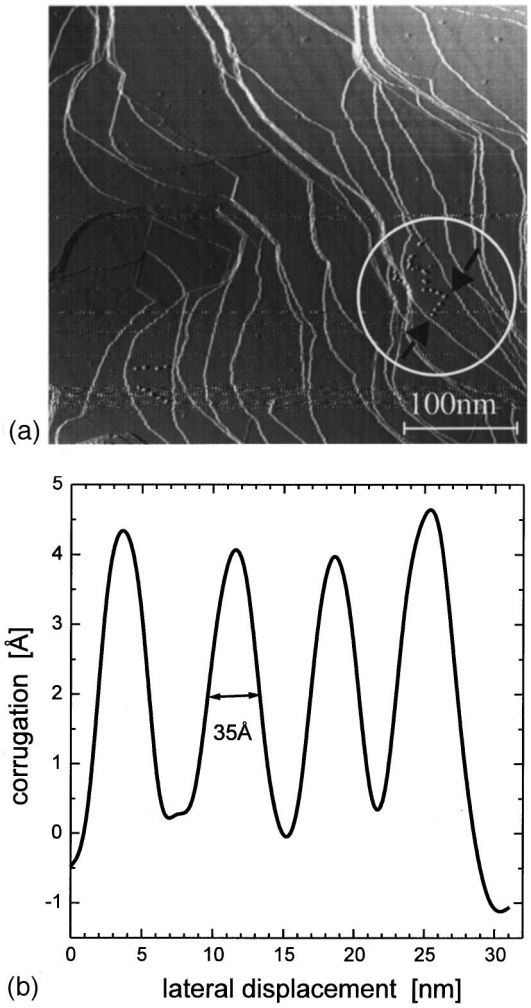

FIG. 10. Topography of a thick smooth Gd film being exposed to 10 L (a). The line section in (b) through clusters marked by arrows in (a) shows that for this different type of sample the clusters possess the same dimension compared to the creation on islands (cf. Fig. 7).

B. Oxygen adsorption

Exposing epitaxial Gd layers to oxygen results in dissociative chemisorption with initial exposure, and is followed by formation of Gd oxide.[9,11,14] The very first step of adsorbing oxygen on Gd islands with the remaining monolayer in between is shown in Fig. 11. In the upper image the exposure amounts to 0.08 L; in the lower one, showing the same area of the sample, it is 0.2 L. It is obvious that in contrast to hydrogen a regular distributed adsorption takes place.

For a demonstration of the differences between oxygen and hydrogen adsorbed on Gd(0001), the surface was covered with small amounts of hydrogen, and subsequently with 0.1-L oxygen. The topography is shown in Fig. 12(a) (70×60 nm^2, $U=-0.7$ V, and $I=1$ nA). The large depressed area on top of the island is caused by hydrogen, the small areas by oxygen. A map of the differential conductivity dI/dU at -0.2 V is presented in Fig. 12(b), showing the reduced local density of states for adsorbed hydrogen at negative voltages [cf. Fig. 6(b)]. Tunneling spectra [see Fig. 12(c)] were recorded on-top of the island for the unaffected Gd surface (curve *A*), the oxygen induced small areas (curve *B*) as well as the hydrogen-affected areas (curve *C*). Spectrum *A* demonstrates that on the undiscovered areas the exchange-split Gd surface state is present. The differential conductivity within the hydrogen-covered area is comparable to the one in Fig. 2. Curve *B* shows that at the oxygen-induced regions the Gd surface state is still present. As will be discussed below in more detail (see Sec. III D), oxygen is adsorbed *below* the Gd surface. This behavior enables the surface state to remain present but with a significantly reduced weight. The further steps in the adsorption process will be discussed below in connection with the adsorption of CO.

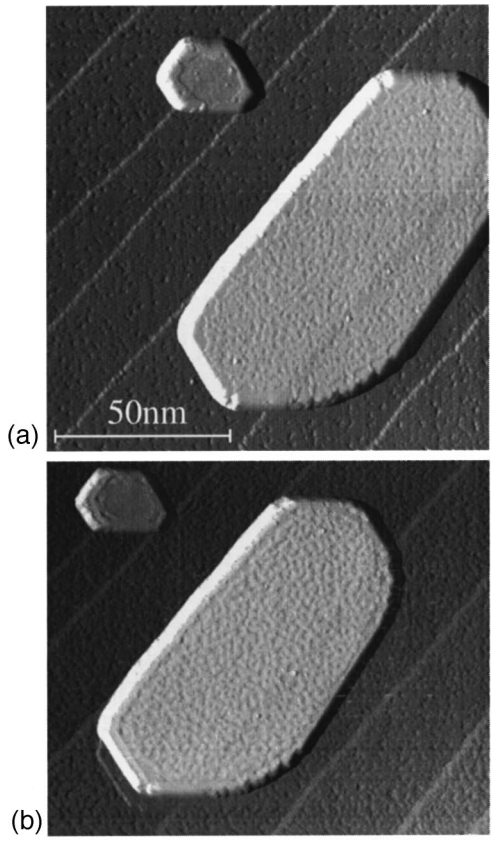

FIG. 11. Topography of a Gd island with the monolayer covering the tungsten substrate between islands exposed to 0.08-L oxygen (a) and 0.2-L oxygen (b).

In the following we turn our attention to oxygen adsorption on the Gd monolayer which is located between the Gd islands. Figure 13(a) shows a detailed image of the monolayer after an exposure of 0.08 L [cf. Fig. 11(a)]. Due to its strong electronegativity the dissociatively adsorbed oxygen molecule is visible as black holes, i.e., adsorbed oxygen is imaged as a depression; this behavior was already found, for example, for O/W(110),[36] and also theoretically predicted.[37] The oxygen overlayer forms an ordered structure. This is not present [Fig. 13(b)] after the additional amount of oxygen on the surface [cf. Fig. 11(b)].

In order to determine the geometrical arrangement, a more detailed image is shown in Fig. 14(a). The adsorption sites of the oxygen atoms form a hexagonal structure which is schematically included into Fig. 14(a). The nearest-neighbor distance amounts to 13 ± 1 Å.

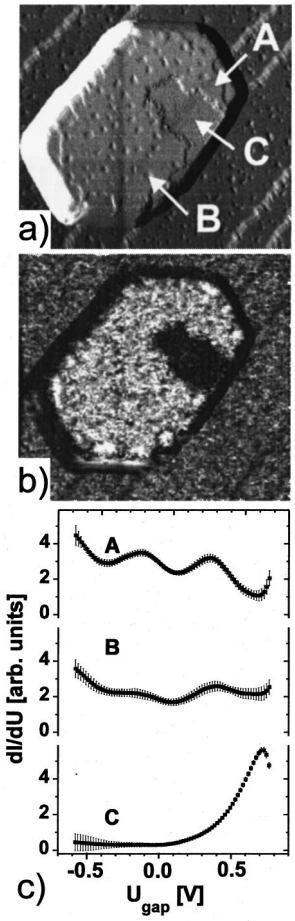

FIG. 12. Gd exposed to a small amount of hydrogen and subsequently to 0.1-L oxygen. (a) Topography (70×60 nm^2, $U=-0.7$ V, and $I=1$ nA). (b) Map of the differential conductivity at -0.2 V. (c) Tunneling spectra of the Gd island for uncovered Gd(0001) (*A*), oxygen-induced small areas (*B*), and the hydrogen-affected area (*C*). These regions are marked in (a).

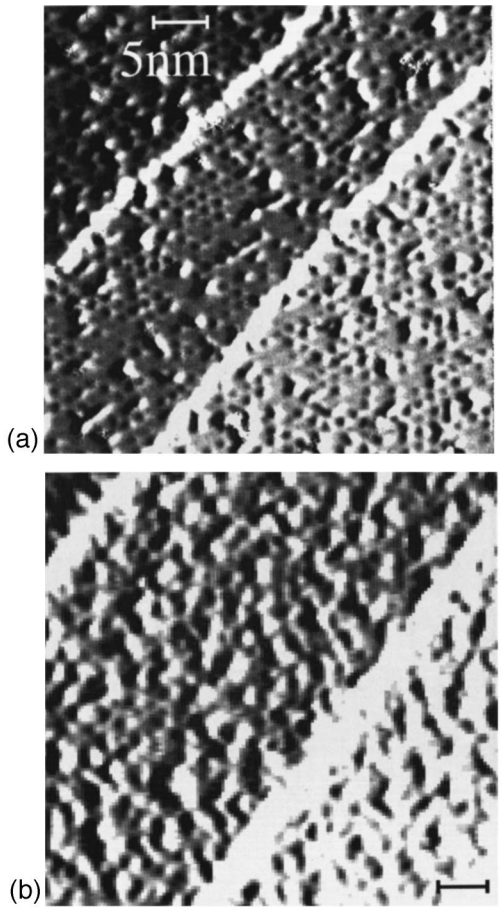

FIG. 13. Topography of the Gd monolayer covering the tungsten substrate between islands exposed to 0.08-L oxygen (a) and 0.2-L oxygen (b). The oyxgen overlayer forms an ordered structure, which is not visible for higher exposures.

The monolayer of Gd which possesses a rectangular 7×14 unit cell[27] is drawn in Fig. 14(b) as light gray balls. The interatomic distances were taken from Ref. 27. Our proposed model of the adsorbate overlayer is included in this figure, which can be attributed to a $(2\sqrt{3}\times2\sqrt{3})R30°$ structure with a nearest-neighbor distance of 12.48 Å, being in excellent agreement. The basic unit cells are shown in dark gray color for the Gd monolayer and in black for the adsorbate system, respectively. It should be noted that the presentation with on-top sites is arbitrary, because we are not able to distinguish between on-top, threefold hollow, and bridge sites based on the STM observations.

C. Gd(0001) exposed to carbon monoxide

The behavior in the adsorption process of CO on Gd(0001) depends strongly on the substrate temperature. Dosing CO to Gd results in a behavior which is shown in Fig. 15. The upper image presents the adsorption of 0.8-L CO at 90 K, the lower one of 0.6-L CO at room temperature. It is obvious that the surfaces of the Gd islands are differently structured. The inset in Fig. 15(b) shows, on the same scale, the Gd surface after an oxygen dosage of 0.08 L. Whereas at low temperature the adsorption seems to occur molecularly, being in agreement, e.g., with investigations concerning the adsorption on Fe(110) (Ref. 38) and on Co(0001),[39] dissociation takes place at 300 K as already shown by Searle *et al.*,[17] and additionally, e.g., for CO on Fe(100) surfaces.[40,41] The similarity between CO and O_2 adsorption is a strong hint of the dissociation of the carbon monoxid molecule at room temperature. Direct evidence will be given by means of photoelectron spectroscopy (see below).

An exposure sequence obtained at room temperature is presented in Fig. 16. For small dosages [1 L in Fig. 16(a)], the surface is relatively smooth, with single localized areas being depressed. For higher exposures [20 L in Fig. 16(b)] the appearance has been changed. As will be discussed below in more detail, the more rough surface points to the creation of carbonate species due to a transformation from CO to CO_2 being caused by Gd_2O_3.

D. Coadsorption of hydrogen and carbon monoxide

In order to obtain a deeper insight into the behavior of catalytic processes, the coadsorption of hydrogen and carbon monoxide was investigated. For this purpose the Gd surface was exposed to small amounts of hydrogen with a subsequent dosage of CO. The basic steps of this process were

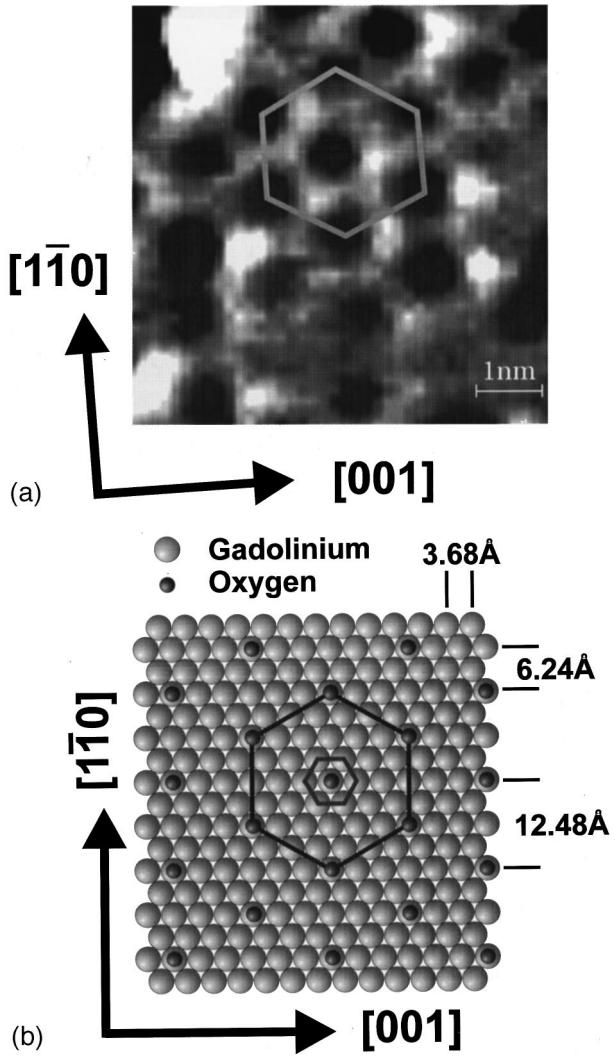

FIG. 14. (a) The same sample as in Fig. 11 with an expanded scale. Adsorbed oxygen is shows as a depression. The adsorption sites of the oyxgen atoms form a hexagonal structure which is schematically included with nearest-neighbor distances of 13 ± 1 Å. The crystallographic axes are in reference to the tungsten substrate. (b) The Gd monolayer possessing a 7×14 unit cell is drawn as light gray balls. Our proposed model of the oxygen overlayer is included by dark gray balls. This structure can be attributed to $(2\sqrt{3}\times2\sqrt{3})R30°$ with a nearest-neighbor distance of 12.48 Å.

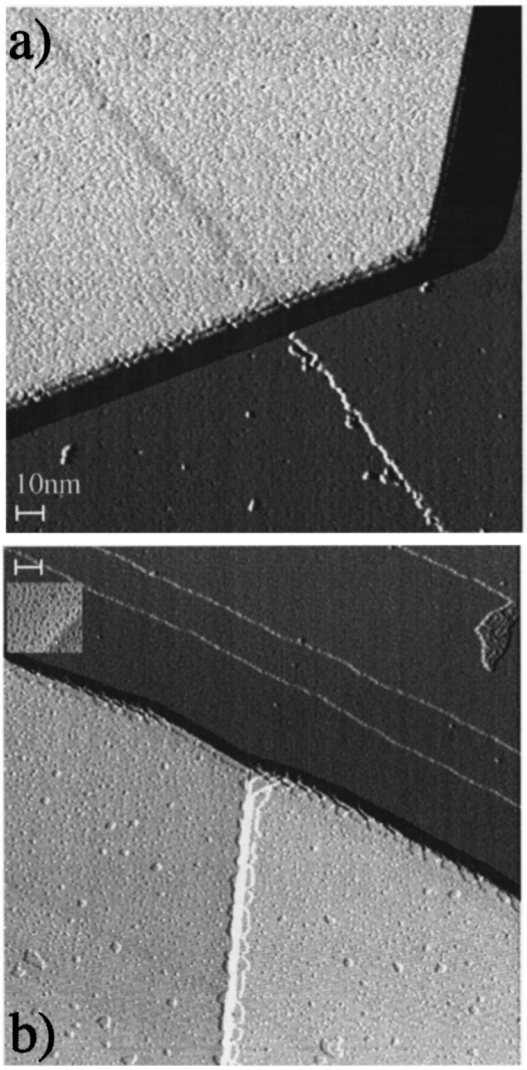

FIG. 15. Topography of Gd islands exposed to CO at 90 K (a) and 293 K (b). It is obvious that the Gd islands are differently structured, pointing to a molecular adsorption at low temperature and to a dissociation of the CO molecules at room temperature.

determined with a sample exposed to 1-L hydrogen being adsorbed on a Gd(0001) surface. This system was exposed to CO with dosages up to 0.81 L. The photoemission spectra are presented in Fig. 17. With increasing CO exposure it can be observed that the Gd surface state near the Fermi level remains nearly unaffected apart from a small decrease in intensity after beginning the CO exposure and a slight shift to higher binding energies. Additionally, the hydrogen induced feature at 4.0-eV binding energy loses intensity, and is absent after 0.81-L CO. In the energy region around 2 eV an additional structure appears with increasing CO exposure; this is not apparent at low coverages.

It was shown[42] for uranium possessing an electronic structure ($[\mathrm{Rn}]5f^36d^17s^2$) related to Gd(0001) ($[\mathrm{Xe}]4f^75d^16s^2$) that after CO adsorption two features appear: one structure at 2.4 eV binding energy is due to C $2p$ emission of UC, and the other one at 2.2 eV by U caused by the existence of oxygen. Therefore, the peak intensities were determined at 2, 2.4, and 4 eV as a function of CO exposure (Fig. 18). The procedure consists of the subtraction of a linear background and a fit with Gaussian functions. It is obvious that the diagram can be classified into four regions, i.e., the adsorption process up to 0.81 L consists of four steps.

At the beginning the hydrogen-induced intensity decreases very quickly, whereas the dissociatively adsorbing CO causes no features in the spectra nor for the C $2p$ state at 2.4 eV nor for the oxygen-caused Gd state at 2.0 eV. In the next step the loss of intensity of the hydrogen state is diminished, the emission of the carbon state begins, and no feature caused by oxygen is present. Step 3 consists of a decrease in the hydrogen-induced intensity with the same slope as in step 1, an increase of the carbon-induced intensity with the same slope as in step 2, and the beginning of oxygen-induced intensity from a Gd state. In step 4 no hydrogen-induced intensity is present, and the carbon- and oxygen-induced states show a strengthened increase of intensity.

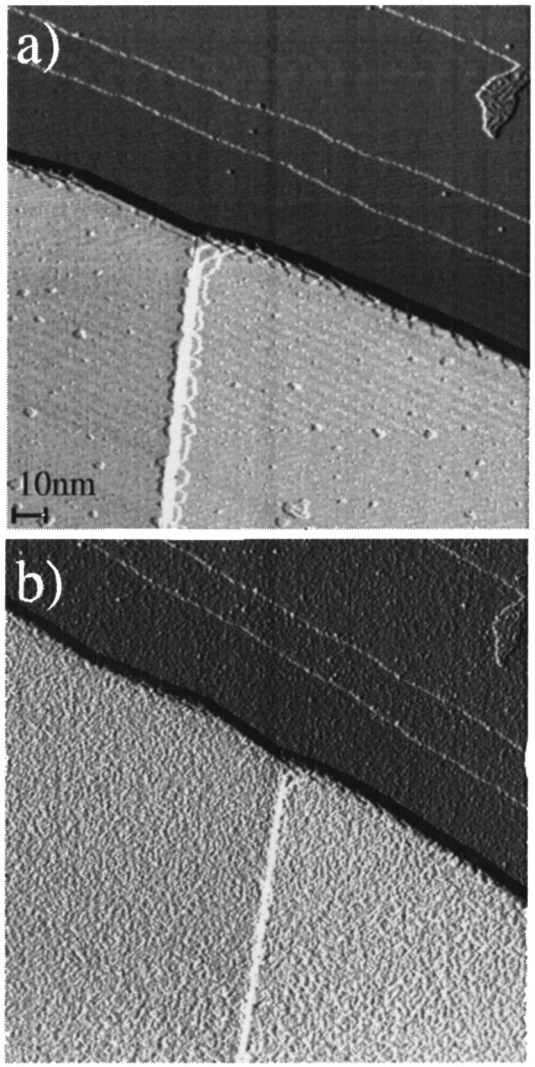

FIG. 16. For small exposures at room temperature [1 L in (a)] the surface looks relatively smooth, whereas for higher dosages [20 L in (b)] it becomes rough.

In the following we want to describe the chemical reactions induced by increasing CO exposure; the superscript gas means gaseous, and ads means adsorbed in any way. In order to obtain a better standard of comparison, all formulas were referenced to an offer of four CO molecules.

During the first step only hydrogen is removed, and no additional species are adsorbed; therefore, all products are gaseous, pointing to the creation of carbon dioxide and methane:

$$\text{Step 1:}\quad 8\mathrm{H}^{\mathrm{ads}}+4\mathrm{CO}^{\mathrm{gas}}\rightarrow 2\mathrm{CO}_2^{\mathrm{gas}}+2\mathrm{CH}_4^{\mathrm{gas}}.$$

The ratio of eight H atoms to four CO molecules for the complete removal of hydrogen can be independently estimated by the following consideration.

It was shown by Li *et al.*[8] that 2-L H_2 are necessary in order to obtain a full coverage of Gd(0001) with an 1×1 overlayer. Due to the dissociative adsorption of H_2, one can estimate, using the Gd lattice constants, that the surface is covered with about eight H atoms per nm^2. In our investigation Gd was exposed to 1-L H_2, i.e., the density amounts to four H atoms per nm^2. The extrapolation in region 1 (see Fig. 18) results in 0.6-L CO being necessary to remove the whole hydrogen. 1-L CO is equivalent to a collision rate of 3.5 molecules/nm^2 (cf. the estimation for hydrogen in Sec. III A), therefore, 0.6-L CO to a rate of about two CO molecules/nm^2. This means that two CO molecules in relation to four H atoms cause a complete removal of hydrogen, as stated above (see reaction scheme of step 1).

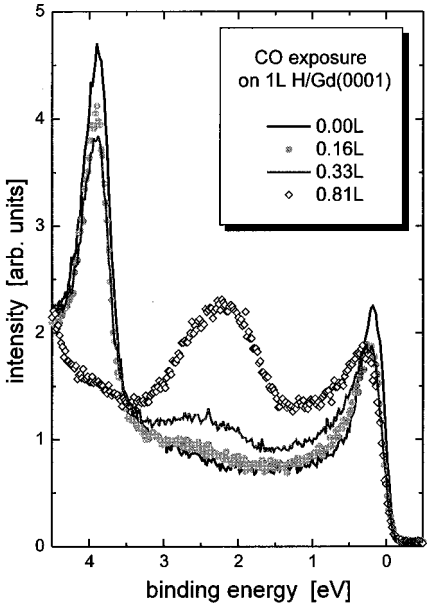

FIG. 17. Photoemission spectra taken in normal emission with $h\nu=16.85$ eV for a smooth Gd film pre-exposed to 1-L hydrogen as a function of CO dosage. With increasing offer, the hydrogen-induced peak at 4-eV binding energy disappears, whereas around 2 eV a broad structure shows an increasing intensity.

In the next step only half a rate of hydrogen is removed as can be seen by the different slope for the H-induced feature in Fig. 18. The additional amount of CO causes the creation

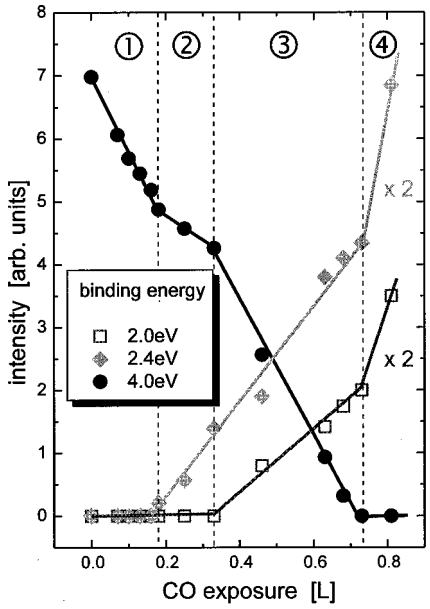

FIG. 18. Peak intensities as a function of CO dosage. The shapes of the curves point to four regions with different behaviors in the adsorption process (the details are discussed in the text).

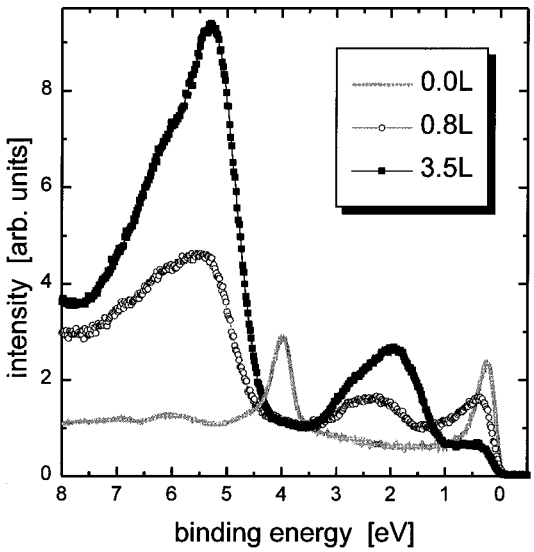

FIG. 19. Photoemission spectra for 0.4-L H/Gd(0001)/W(110) with increasing CO dosage (cf. Fig. 17). The broad peak around 6-eV binding energy is due to oxygen being adsorbed below the surface. The double-peaked structure for higher dosages points to the formation of Gd_2O_3. This is in agreement with the drastically decreased intensity near the Fermi level.

of carbon on or near the surface but no oxygen atom is adsorbed. The reaction can therefore be written as

$$\text{Step 2:}\quad \mathrm{Gd}+4\mathrm{H}^{\mathrm{ads}}+4\mathrm{CO}^{\mathrm{gas}}\rightarrow 2\mathrm{CO}_2^{\mathrm{gas}}+\mathrm{CH}_4^{\mathrm{gas}}+\mathrm{GdC}^{\mathrm{ads}}.$$

This formation of Gd(0001) carbide was also observed for U exposed to CO.[42]

During further exposure, hydrogen is removed with the same rate compared to the beginning. The rate of carbon creation remains constant, but now oxygen is adsorbed creating a subsurface oxide and causes emission from Gd^{2+} states, as already discussed for oxygen adsorbed on Gd.[9] This reaction can be described by

$$\text{Step 3:}\quad 3\mathrm{Gd}+8\mathrm{H}^{\mathrm{ads}}+4\mathrm{CO}^{\mathrm{gas}}\rightarrow \mathrm{CO}_2^{\mathrm{gas}}+2\mathrm{CH}_4^{\mathrm{gas}}+\mathrm{GdC}^{\mathrm{ads}}+2\mathrm{GdO}^{\mathrm{ads}}.$$

At the end of step 3 the *whole* amount of hydrogen has been removed from the surface.

The next step is characterized by the creation of carbon and Gd suboxide of the same type as in the former steps:

$$\text{Step 4:}\quad 4\mathrm{Gd}+4\mathrm{CO}^{\mathrm{gas}}\rightarrow 4\mathrm{GdC}^{\mathrm{ads}}+4\mathrm{GdO}^{\mathrm{ads}},$$

as being obvious due to the strengthened increase in the peak intensities around 2 eV binding energy.

In order to determine the influence of higher offers of CO, the Gd film was exposed to 0.4-L hydrogen with subsequent CO dosage by up to 3.5-L. These spectra are presented in Fig. 19. In the low-coverage regime the results are comparable to the system discussed above. In contrast, the spectrum for 3.5-L CO looks significantly different. No feature at the Fermi level is present any longer, and the one around 2-eV binding energy shows a two-peak structure. The change in the electronic properties is additionally visible in the energy range of O $2p$ states around 6-eV binding energy. Whereas for the low offer a single broad peak can be observed, pointing to oxygen in the Gd subsurface oxide,[14] at higher exposures a double-peaked structure appears which is characteristic of Gd_2O_3.[9] It is known[43] that sesquioxides of rare-earth metals R_2O_3 are a catalyst for the transformation of CO to CO_2. These carbonates are stable at the surface. Gd in Gd_2O_3 possesses the oxidation stage Gd^{3+}, losing all valence electrons, as seen in the drastic decrease in intensity near the Fermi level. We therefore attribute the significantly different structure around 2 eV binding energy to emission of this carbonate species, as already supposed by Searle *et al.*[17] Taking into account these considerations, the further step in the process can be described by

$$\text{Step 5:}\quad 6\mathrm{GdO}+4\mathrm{CO}^{\mathrm{gas}}\rightarrow 2\mathrm{GdC}^{\mathrm{ads}}+2(\mathrm{Gd_2O_3}\times\mathrm{CO_2})^{\mathrm{ads}}.$$

It should be noted that a part of the carbonate species may be desorbed as CO_2^{gas}.

The peak intensities as a function of CO exposure are given in Fig. 20(a). It is obvious that the same mechanism takes place. The corresponding STM images taken for 0- and 0.6-L CO, shown with an expanded scale in Fig. 21, demonstrate the removal of hydrogen. Above 1 L an additional regime 5 occurs. This is illustrated in Fig. 20(b) by an expanded scale. The corresponding STM image is given for a CO dosage of 3.5 L. The increased intensity becomes reduced compared to region 4.

The ''visualization'' of this process was carried out via scanning tunneling microscopy. For this purpose Gd islands with hcp(0001) surfaces were exposed to 0.4-L hydrogen. The affected areas can be seen in Fig. 21(a) [cf. additionally Fig. 20(a)]. To this system, CO was subsequently dosed. After an offer of 0.6 L no collapsed areas are observable [see Fig. 21(b)] pointing to no remaining hydrogen at the surface. At this amount region 4 is reached, and the complete hydrogen adsorbate is removed by CO. The single areas with a reduced apparent height are caused by contamination during the Gd formation. They are also observable in Fig. 21(a). Figure 21(c) shows the sample which was exposed to 3.5-L CO. In step 5, carbonate species are created which cause this rough looking surface.

This direct comparison, i.e., the *visualization* of the changes in the electronic properties caused by chemical reactions at the surface, expresses the advantage of the combination of photoelectron spectroscopy with scanning tunneling microscopy and spectroscopy.

IV. SUMMARY

In summary we have determined the electronic structure of hydrogen, oxygen, and carbon monoxide on Gd(0001) and studied the development of the adsorption processes. Scanning tunneling microscopy and spectroscopy allow due to its high spatial resolution the observation, i.e., the *visualization* of the spreading of the adsorption. For hydrogen, it was found that the adsorption occurs in two steps. It is initiated by surface imperfections. Starting from these nucleation centers, a domainlike spreading is present which is strongly pinned at surface steps acting as domain boundaries.

Oxygen on the Gd monolayer possesses an ordered struc-

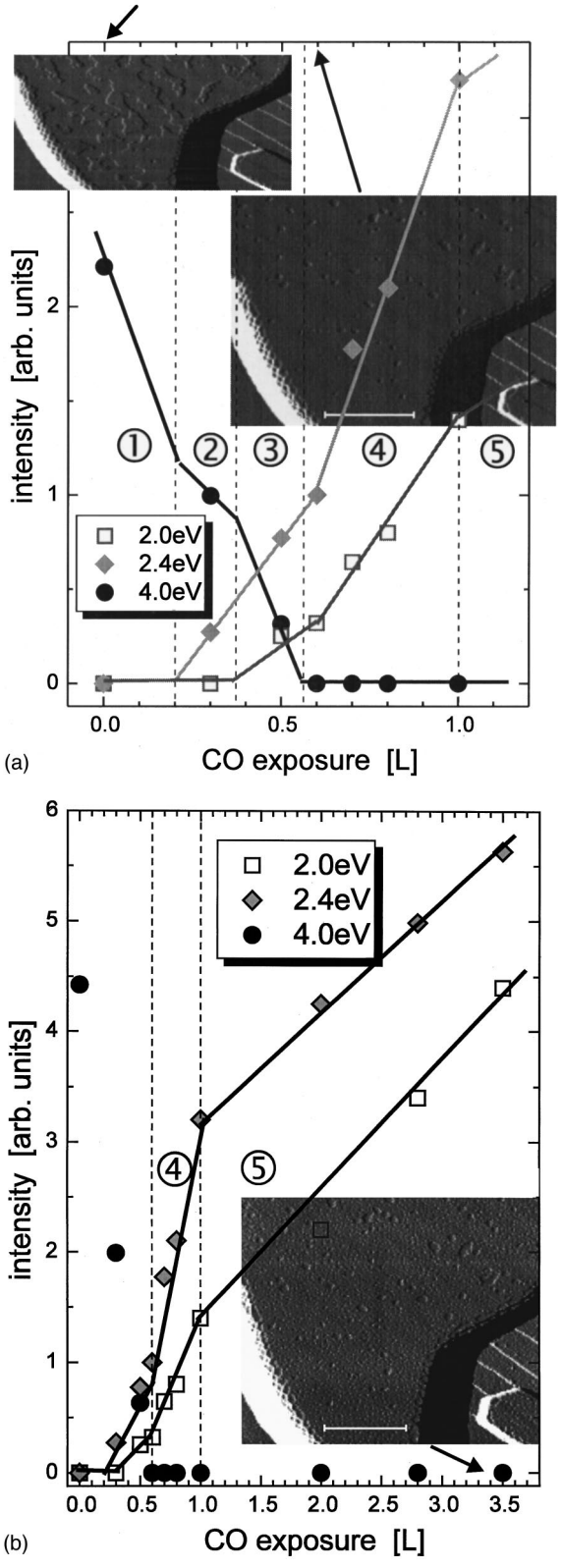

FIG. 20. (a) Intensities of the hydrogen-induced structure at 4 eV, the oxygen-induced Gd state at 2.0 eV, and the C $2p$ state at 2.4 eV as a function of CO dosage. The adsorption process can be divided into five steps. The corresponding topography is shown for 0- and 0.6-L CO as insets. The removal of hydrogen can be observed due to the reappearance of the Gd surface state. (b) Same as in (a), but for higher coverages. The corresponding STM image is taken for a dosage of 3.5-L CO.

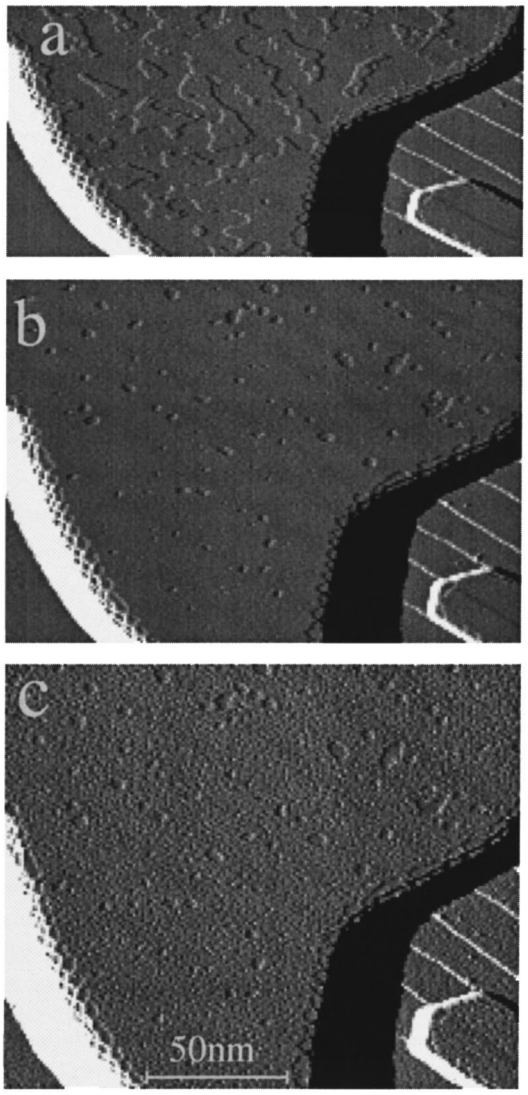

FIG. 21. Enlarged images of the STM pictures in Fig. 20 taken at CO dosages of 0 L (a), 0.6 L (b), and 3.5 L (c).

ture which could be determined to be $(2\sqrt{3}\times 2\sqrt{3})R30°$. Carbon monoxide adsorbs molecularly at low temperatures and dissociatively at room temperature.

The adsorption process of a hydrogen covered Gd film being exposed to carbon monoxide consists of five steps. At the beginning the total amount of adsorbed hydrogen atoms is removed. In the intermediate regime, carbon and oxygen is adsorbed at or near the surface. The last step demonstrates the oxidation to Gd_2O_3 acting as a catalyst for the transformation of CO to CO_2, which creates stable carbonate species at the surface. This formation also occurs for the adsorption of oxygen and carbon monoxide.

ACKNOWLEDGMENTS

We acknowledge financial support by the DFG through Grant No. Wi 1277/4-1, and the Graduiertenkolleg ''Physik nanostrukturierter Festkörper.''

[1] D. Weller, S.F. Alvarado, W. Gudat, K. Schröder, and M. Campagna, Phys. Rev. Lett. **54**, 1555 (1985).
[2] E. Vescovo, C. Carbone, and O. Rader, Phys. Rev. B **48**, 7731 (1993).
[3] D. Li, J. Pearson, S.D. Bader, D.N. McIlroy, C. Waldfried, and P.A. Dowben, Phys. Rev. B **51**, 13 895 (1995).
[4] R. Wu, C. Li, A.J. Freeman, and C.L. Fu, Phys. Rev. B **44**, 9400 (1991).
[5] G.A. Mulhollan, K. Garrison, and J.L. Erskine, Phys. Rev. Lett. **69**, 3240 (1992).
[6] H. Tang, D. Weller, T.G. Walker, J.C. Scott, C. Chappert, H. Hopster, A.W. Pang, D.S. Dessau, and D.P. Pappas, Phys. Rev. Lett. **71**, 444 (1993).
[7] A.W. Pang, A. Berger, and H. Hopster, Phys. Rev. B **50**, 6457 (1994).
[8] D. Li, J. Zhang, P.A. Dowben, and M. Onellion, Phys. Rev. B **48**, 5612 (1993).
[9] K. Wandelt and C.R. Brundle, Surf. Sci. **157**, 162 (1985).
[10] D. Weller, S.F. Alvarado, M. Campagna, W. Gudat, and D.D. Sarma, J. Less-Common Met. **111**, 277 (1985).
[11] D. Weller and D.D. Sarma, Surf. Sci. **171**, L425 (1986).
[12] E. Vescovo, O. Rader, T. Kachel, U. Alkemper, and C. Carbone, Phys. Rev. B **47**, 13 899 (1993).
[13] J.E. Ortega, F.J. Himpsel, D. Li, and P.A. Dowben, Solid State Commun. **91**, 807 (1994).
[14] J. Zhang, P.A. Dowben, D. Li, and M. Onellion, Surf. Sci. **329**, 177 (1995).
[15] M. Getzlaff, J. Paul, J. Bansmann, Ch. Ostertag, G.H. Fecher, and G. Schönhense, Surf. Sci. **352–254**, 123 (1996).
[16] D.N. McIlroy, C. Waldfried, D. Li, J. Pearson, S.D. Bader, D.-J. Huang, P.D. Johnson, R.F. Sabiryanov, S.S. Jaswal, and P.A. Dowben, Phys. Rev. Lett. **76**, 2802 (1996).
[17] C. Searle, R.I.R. Blyth, R.G. White, N.P. Tucker, M.H. Lee, and S.D. Barrett, J. Synchrotron Radiat. **2**, 312 (1995).
[18] D. Li, C.W. Hutchings, P.A. Dowben, C. Hwang, R.-T. Wu, M. Onellion, A.B. Andrews, and J.L. Erskine, J. Magn. Magn. Mater. **99**, 85 (1991).
[19] T. Trappmann, M. Gajdzik, C. Sürgers, and H.v. Löhneysen, Europhys. Lett. **39**, 159 (1997).
[20] M. Gajdzik, T. Trappmann, C. Sürgers, and H.v. Löhneysen, Phys. Rev. B **57**, 3525 (1998).
[21] R. Kalinowski, L.T. Baczewski, A. Wawro, C. Meyer, and J. Raułuszkiewicz, Acta Phys. Pol. A **93** 409 (1999).
[22] S.C. Wu, H. Li, Y.S. Li, D. Tian, J. Quinn, F. Jona, and D. Fort, Phys. Rev. B **44**, 13 720 (1991).
[23] Ch. Ostertag, J. Paul, N.A. Cherepkov, A. Oelsner, G.H. Fecher, and G. Schönhense, Surf. Sci. **377–379**, 427 (1997).
[24] C. Hwang, J.W. Lee, S.T. Kim, D.H. Lee, and M. Onellion, Solid State Commun. **103**, 229 (1997).
[25] G. Schönhense and U. Heinzmann, J. Phys. E **16**, 74 (1983).
[26] A. Aspelmeier, F. Gerhardter, and K. Baberschke, J. Magn. Magn. Mater. **132**, 22 (1994).
[27] E.D. Tober, R.X. Ynzunza, C. Westphal, and C.S. Fadley, Phys. Rev. B **53**, 5444 (1996).
[28] M. Getzlaff, M. Bode, S. Heinze, R. Pascal, and R. Wiesendanger, J. Magn. Magn. Mater. **184**, 155 (1998).
[29] B. Kim, A.B. Andrews, J.L. Erskine, K.J. Kim, and B.N. Harmon, Phys. Rev. Lett. **68**, 1931 (1992).
[30] M. Donath, B. Gubanka, and F. Passek, Phys. Rev. Lett. **77**, 5138 (1996).
[31] D. Weller and S.F. Alvarado, J. Appl. Phys. **59**, 2908 (1986).
[32] M. Bode, M. Getzlaff, S. Heinze, R. Pascal, and R. Wiesendanger, Appl. Phys. A: Mater. Sci. Process. **66**, S121 (1998).
[33] R.G. White, M.H. Lee, N.P. Tucker, S.D. Barrett, and P.W. Murray, Phys. Rev. B **56**, R10071 (1997).
[34] D. Menzel and J.C. Fuggle, Surf. Sci. **74**, 321 (1978).
[35] K.B. Ray, X. Pan, and E.W. Plummer, Surf. Sci. **285**, 66 (1993).
[36] K.E. Johnson, R.J. Wilson, and S. Chiang, Phys. Rev. Lett. **71**, 1055 (1993).
[37] N.D. Lang, Comments Condens. Matter Phys. **14**, 253 (1989).
[38] M. Getzlaff, J. Bansmann, C. Westphal, and G. Schönhense, J. Magn. Magn. Mater. **104-107**, 1781 (1992).
[39] M. Getzlaff, J. Bansmann, and G. Schönhense, J. Chem. Phys. **103**, 6691 (1995).
[40] T.N. Rhodin and C.F. Brucker, Solid State Commun. **23**, 275 (1977).
[41] M. Getzlaff, J. Bansmann, and G. Schönhense, Fresenius J. Anal. Chem. **353**, 748 (1995).
[42] T. Gouder, C.A. Colmenares, J.R. Naegele, J.C. Spirlet, and J. Verbist, Surf. Sci. **264**, 354 (1992).
[43] F. P. Netzer and E. Bertel, in *Handbook on the Physics and Chemistry of Rare Earths*, edited by K. A. Gschneidner and L. Eyring (North-Holland, Amsterdam, 1982), Vol. 5, p. 217.